ARTICLE OPEN

Check for updates

Evaluation of in vivo staging of amyloid deposition in cognitively unimpaired elderly aged 78–94

Malgorzata M. Michalowska[1,2,3], Karl Herholz[1,4,5], Rainer Hinz[1], Chinenye Amadi[1,4], Lynn McInnes[6], Jose M. Anton-Rodriguez[1,7], Thomas K. Karikari[8,9], Kaj Blennow[8,10], Henrik Zetterberg[8,10,11,12,13], Nicholas J. Ashton[8,14,15,16], Neil Pendleton[4] and Stephen F. Carter[1,17]✉

Amyloid-beta (Aβ) deposition is common in cognitively unimpaired (CU) elderly >85 years. This study investigated amyloid distribution and evaluated three published in vivo amyloid-PET staging schemes from a cognitively unimpaired (CU) cohort aged 84.9 ± 4.3 years ($n = 75$). SUV-based principal component analysis (PCA) was applied to ^{18}F-flutemetamol PET data to determine an unbiased regional covariance pattern of tracer uptake across grey matter regions. PET staging schemes were applied to the data and compared to the PCA output. Concentration of p-tau181 was measured in blood plasma. The PCA revealed three distinct components accounting for 91.2% of total SUV variance. PC1 driven by the large common variance of uptake in neocortical and striatal regions was significantly positively correlated with global SUVRs, APOE4 status and p-tau181 concentration. PC2 represented mainly non-specific uptake in typical amyloid-PET reference regions, and PC3 the occipital lobe. Application of the staging schemes demonstrated that the majority of the CU cohort (up to 93%) were classified as having pathological amount and distribution of Aβ. Good correspondence existed between binary (+/−) classification and later amyloid stages, however, substantial differences existed between schemes for low stages with 8–17% of individuals being unstageable, i.e., not following the sequential progression of Aβ deposition. In spite of the difference in staging outcomes there was broad spatial overlap between earlier stages and PC1, most prominently in default mode network regions. This study critically evaluated the utility of in vivo amyloid staging from a single PET scan in CU elderly and found that early amyloid stages could not be consistently classified. The majority of the cohort had pathological Aβ, thus, it remains an open topic what constitutes abnormal brain Aβ in the oldest-old and what is the best method to determine that.

Molecular Psychiatry (2022) 27:4335–4342; https://doi.org/10.1038/s41380-022-01685-6

INTRODUCTION

Deposition of amyloid plaques is an early event in Alzheimer's disease (AD) pathogenesis [1]. Deposition of amyloid-beta (Aβ) is also observed in up to 38% of cognitively unimpaired (CU) older individuals at age 85 [2] and up to 76% in those carrying at least one copy of the ε4 allele of the apolipoprotein E gene (APOE4). However, it is unclear whether this represents an early stage of AD ultimately leading to dementia, or whether it represents a benign age-associated condition.

Positron emission tomography (PET) imaging allows in vivo visualisation and quantification of brain Aβ [3, 4]. Staging schemes based on post mortem histology and amyloid imaging research across the AD spectrum, including individuals with preclinical AD, suggest a downward spreading pattern starting in the neocortex and progressing toward the striatum [5, 6]. Thal et al. estimated neuropathological Aβ-phases [5] by using thresholds based on standardised uptake value ratios (SUVRs) for neocortex and caudate nucleus [7]. Grothe et al. described [8] and longitudinally validated [9] four stages of regional amyloid deposition on ^{18}F-florbetapir PET scans in CU individuals, with partial replication in patients with subjective memory impairment [10]. Mattsson et al. defined three stages based on regional longitudinal cortical amyloid progression rates informed by CSF biomarkers [11] (an extended discussion of Thal's, Grothe's and Mattsson's staging schemes can be found in the Supplementary Information). While there is evidence of good correspondence between PET-based

[1]Wolfson Molecular Imaging Centre, University of Manchester, Manchester, UK. [2]Department of Neuropsychology and Psychopharmacology, Maastricht University, Maastricht, The Netherlands. [3]Division of Clinical Geriatrics, Center for Alzheimer Research, Department of Neurobiology, Care Sciences and Society, Karolinska Institutet, Stockholm, Sweden. [4]Division of Neuroscience and Experimental Psychology, University of Manchester, Manchester, UK. [5]Sheffield Institute for Translational Neuroscience, University of Sheffield, Sheffield, UK. [6]Department of Psychology, Faculty of Health and Life Sciences, Northumbria University, Newcastle upon Tyne, UK. [7]Christie Medical Physics and Engineering, The Christie NHS Foundation Trust, Manchester, UK. [8]Department of Psychiatry and Neurochemistry, Institute of Neuroscience and Physiology, The Sahlgrenska Academy at the University of Gothenburg, Mölndal, Sweden. [9]Department of Psychiatry, University of Pittsburgh, Pittsburgh, PA, USA. [10]Clinical Neurochemistry Laboratory, Sahlgrenska University Hospital, Mölndal, Sweden. [11]Department of Neurodegenerative Disease, UCL Institute of Neurology, Queen Square, London, UK. [12]UK Dementia Research Institute at UCL, London, UK. [13]Hong Kong Center for Neurodegenerative Diseases, Clear Water Bay, Hong Kong, China. [14]King's College London, Institute of Psychiatry, Psychology and Neuroscience Maurice Wohl Institute Clinical Neuroscience Institute, London, UK. [15]NIHR Biomedical Research Centre for Mental Health and Biomedical Research Unit for Dementia at South London and Maudsley NHS Foundation, London, UK. [16]Centre for Age-Related Medicine, Stavanger University Hospital, Stavanger, Norway. [17]Department of Psychiatry, University of Cambridge, Cambridge, UK. ✉email: Stephen.f.carter@manchester.ac.uk

Received: 28 January 2022 Revised: 27 May 2022 Accepted: 27 June 2022
Published online: 20 July 2022

and neuropathological staging in patients with MCI or dementia, discrepant findings were observed in CU controls for low and moderate severity amyloid pathology [12].

Neuropathological studies in CU aged above 80 years [13] or centenarians [14] found little if any relation of cross-sectional cognitive function or previous decline with Aβ staging. Thus, the concept of describing the progression of AD by amyloid staging does not seem applicable in these individuals, who may exhibit resilience against any detrimental effects of amyloid. The regional distribution of amyloid deposits in these people may not be aligned with the regional progression pattern rendering them unstageable. As amyloid-PET is providing quantitative values of amyloid tracer uptake, multivariate techniques such as principal component analysis (PCA) can be used to describe distribution patterns [15]. This has previously been used to study the effects of ageing on cerebral glucose metabolism [16], to distinguish between dementia types [17], with amyloid-PET for discrimination between AD patients and controls [18] or for generating templates for spatial processing [19].

Surviving participants from the Newcastle and Manchester Ageing Cohort [20] have now reached 80 years of age and above. This unique, well-characterised elderly population is, on average, at least 10 years older than many previously published studies. Cognitively unimpaired volunteers from this cohort were included to investigate regional amyloid distribution and to determine associations with cognitive function and established confounding risk factors for amyloid deposition, including age and APOE4 presence. PCA was used to describe the regional amyloid deposition pattern without a priori hypotheses. Published in vivo amyloid-PET staging schemes [8, 9, 11] were also tested to determine if they translate to this CU age group.

METHODS

Participants

Data were acquired from 75 CU elderly, who were part of the PreclinAD study from the European Medical Information Framework for AD [21]. Detailed inclusion and exclusion criteria are outlined in the Supplementary Information. This study was approved by the Greater Manchester South Research Ethics Committee (ref: 14/NW/011) and participants provided written informed consent.

Collected demographic and clinical data

Data on age, years of education, and APOE genotypes were collected [21]. Scores from the Mini-Mental State Examination, Addenbrooke's Cognitive Examination-Revised (ACE-R), CERAD, Rey Auditory Learning Test (RAVLT), and Rey Complex Figure Delayed Test (RCFT Delayed) were collected for an overview of cognitive performance. Based on the APOE genotypes, participants were dichotomised into individuals carrying at least one copy of the ε4 allele (APOE4+) and APOE4 non-carriers (APOE4−).

MRI and PET data acquisition

MRI was performed on a 3T Philips Achieva scanner with a 32-channel head coil including a 3D-T1 with sagittal turbo field echo sequence (1.0 mm isotropic voxels, repetition time = 7.9 ms, echo time = 4.5 ms, flip angle = 8 degrees) for image processing. Radiosynthesis of ^{18}F-flutemetamol was performed at the Wolfson Molecular Imaging Centre, University of Manchester. All PET data were acquired on a high-resolution research tomograph (Siemens/CTI, Knoxville, Tennessee, USA). Following an intravenous injection of 185.07 ± 10.5 MBq ^{18}F-flutemetamol, PET data were acquired from 90–110 min. A 7 min transmission scan using a 137Cs point source was acquired for attenuation and scatter correction [22, 23]. PET images were realigned to correct for inter-frame motion and reconstructed with an implementation of 3D iterative ordinary Poisson ordered subset expectation maximisation with 12 iterations, 16 subsets and resolution modelling [24–27] using 1.22 mm isotropic voxels. A post-reconstruction Gaussian filter of 4 mm FWHM was used to reduce noise [21].

Blood plasma p-tau181

Blood samples were collected and frozen on the same day as the PET scan. Plasma p-tau181 concentration was measured using in-house Single molecule array (Simoa) methods on Simoa HD-X instruments (Quanterix, Billerica, MA, USA) at the University of Gothenburg. Methods are described in the Supplementary Information and detailed elsewhere [28, 29]. No blood samples were acquired for 1 participant and 1 sample was excluded due to being >3 SD outside the cohort mean, leaving 73 p-tau181 samples for analysis. To dichotomise the blood plasma p-tau into T−/T+ groups, a cut-off of 17.7 pg/ml was used [30].

Data processing

Using SPM12 (Statistical Parametric Mapping, Wellcome Trust Centre for Neuroimaging, UCL, UK) with MATLAB R2019b (The MathWorks, Inc., Natick, MA, USA) PET images were coregistered and resliced to the T1-weighted image by rigid body transformation. The T1 images were then segmented into grey matter (GM), white matter (WM), and cerebrospinal fluid (CSF). The Hammers n30r85 probabilistic atlas [31] was inversely warped into native T1 space. GM binary images were created by thresholding the segmented GM images at 0.5. A GM atlas was created by multiplying the GM binary image with the inversely warped Hammers atlas and then used to sample the coregistered PET images, generating mean kBq/ml for 85 brain regions. Harvard-Oxford and Desikan-Killiany (freesurfer) [32] atlases were inverse warped into native T1 space and restricted to GM voxels for each participant so that the percentage of suprathreshold amyloid within the stages established by Grothe [8] and Mattsson [11] could be determined.

For improved spatial accuracy of basal ganglia region definition, Diffeomorphic Anatomical Registration Through Exponentiated Algebra (DARTEL) was added [33]. The standard DARTEL pipeline from SPM was used with segmented GM, WM, and CSF images to transform PET images and the Hammers atlas into the study-specific DARTEL template space, where putamen and caudate nucleus were manually delineated in the axial plane.

To avoid overrepresentation of smaller regions, the orbitofrontal cortex regions (straight gyrus, anterior orbital gyrus, medial orbital gyrus, lateral orbital gyrus, posterior orbital gyrus) were merged, as well as small basal ganglia regions (nucleus accumbens, substantia nigra, pallidum). Thus, standardised uptake values (SUVs) of 67 GM regions entered into the PCA.

A non-standard centiloid (CL) pipeline was adopted following the directions specified in Klunk et al. [34] with Hammers' atlas cerebellar GM as reference region as outlined in the Supplementary Information (Supplementary Figs. 1–3). Amyloid positivity (Aβ+) was determined globally and regionally with published cut-offs established with in vivo [35] and post mortem data [36]. Global positivity was defined as >29 CL (>1.48 SUVR) and within stage regions [8, 11] >12 CL (>1.31 SUVR) was considered positive. Between 12–29 CL is classed as the "grey zone". For Aβ phase estimates from Thal [7], the specific, published cut-offs, with pons as reference region, were used.

Statistical analyses

Statistical analyses were performed with SPSS 25 (SPSS Chicago, IL, USA) using a $p < 0.05$ threshold of statistical significance. Independent *t*-tests compared demographic and clinical data between groups (with adjustment for unequal group size where appropriate). Multiple regression assessed whether cognitive scores are predicted by age, APOE4, or education years. Amyloid distribution across 67 GM regions was examined by entering SUVs into a PCA, to uncover possible interrelations between brain regions [37]. Regions loading highly on the same principle component (PC) would indicate comparable ^{18}F-flutemetamol retention, thus allowing for a regional depiction of amyloid deposition. SUVs instead of SUVRs permitted a reference region-independent representation of covariation of amyloid accumulation. The suitability of the data for PCA was tested with the Kaiser-Meyer-Olkin (KMO) test. The correlation matrix was assessed to ensure that the correlations between the regional SUVs are significant and exceed $r = 0.30$. Components were extracted with a criterion of an eigenvalue above 1. An orthogonal varimax rotation ensured that PCs were uncorrelated with each other, thus improving their interpretability. Finally, each individual's regression-based component loading was saved for extracted PCs.

The effects of APOE4, age, and years of education on regional amyloid deposition (expressed by individual PC loadings) were examined with Pearson partial correlations. For exploratory purposes, cognitive measures were correlated with the PC loadings, adjusting for APOE4, age, and years of education years. The individual loadings were also correlated with CL/SUVRs. The percentage of suprathreshold amyloid deposition was reported according to the staging schemes discussed above [7, 8, 11].

Table 1. Characteristics of the cohort.

Measure	Overall	Aβ−	Aβ+	APOE4−	APOE4+
Age (years)	84.9 ± 4.27	85.4 ± 4.08	84.4 ± 4.44	85.5 ± 4.26	82.7 ± 3.67[a]
Sex (F/M)	58/17	25/10	33/7	43/14	15/3
Education (years)	14.2 ± 2.98	15.1 ± 3.17	13.3 ± 2.55	14.3 ± 3.18	13.9 ± 2.26
MMSE (/30)	28.8 ± 1.24	29 ± .93	28.6 ± 1.41	28.8 ± 1.13	28.7 ± 1.53
ACE-R total (/100)	92.68 ± 4.91	93.11 ± 4.35	92.3 ± 5.39	92.6 ± 4.86	92.9 ± 5.21
ACE-R Memory (/26)	23.2 ± 2.83	23.1 ± 2.71	23.3 ± 2.95	23.2 ± 2.97	23.2 ± 2.39
CERAD Delayed (/10)	8.15 ± 1.54	7.83 ± 1.63	8.43 ± 1.41	8.18 ± 1.53	8.06 ± 1.58
RAVLT Delayed (/15)	10.6 ± 3.32	10.2 ± 3.39	11.0 ± 3.25	10.7 ± 3.21	10.4 ± 3.72
RCFT Delayed (/36)	14.9 ± 6.17[b]	15.0 ± 5.24	14.8 ± 6.95	14.0 ± 5.78	17.6 ± 6.7[a]
p-tau181 (pg/ml; $n = 73$)	16.3 ± 5.64	14.7 ± 5.14	17.7 ± 5.72[c]	15.8 ± 5.82	17.9 ± 4.79
	***n* (%)**	***n* (%)**	***n* (%)**	***n* (%)**	***n* (%)**
Aβ+ (>29 CL\1.48 SUVR)	40 (53.3)	35 (46.7)	40 (53.3)	26 (45.6)	14 (77.8)
APOE4−	57 (76)	31 (88.6)	26 (65)	57 (100)	–
APOE4+	18 (24.3)	4 (11.4)	14 (35)	–	18 (100)
APOE E2/E4	3 (4.1)	1 (2.9)	2 (5)	–	3 (16.7)
APOE E3/E4	14 (19.2)	3 (8.6)	11 (27.5)	–	14 (77.8)
APOE E4/E4	1 (1.4)	–	1 (2.5)	–	1 (5.6)
Middle-old (78–84 years)	38 (50.7)	15 (42.9)	23 (57.5)	25 (43.9)	13 (72.2)
Oldest-old (≥85 years)	37 (49.3)	20 (57.1)	17 (42.5)	32 (56.1)	5 (27.8)

Values are mean ± standard deviation, or number of participants in a subset of the sample (*n*).
MMSE Mini-Mental State Examination, *ACE-R* Addenbrooke's Cognitive Examination-Revised, *CERAD* Consortium to Establish a Registry for Alzheimer's Disease, *RAVLT* Rey Auditory Learning Test, *RCFT* Rey Complex Figure Test, *CL* centiloid, *APOE* apolipoprotein E.
[a]Significant difference ($p < 0.05$) between APOE4− and APOE4+ according to the independent samples *t*-test.
[b]Significant difference ($p < 0.05$) between middle- and oldest-old individuals according to the independent samples *t*-test.
[c]Significant difference ($p < 0.02$) between Aβ− and Aβ+ individuals according to the independent samples *t*-test.

RESULTS

Demographic characteristics and cognition

Table 1 summarises the cohort. Significant differences were found between APOE4− and APOE4+ in terms age and RCFT delayed. Delayed RCFT was significantly different between middle-old and oldest-old individuals (see Supplementary Table 1). Multiple regression predicting RCFT-delayed from APOE4 status and age was significant ($F_{(2,\ 72)} = 8.42$, $p = 0.001$, $R^2 = 0.17$) but only age contributed to the model significantly ($B = -0.53$, $p = 0.001$). Total ACE-R scores were significantly correlated with years of education, accounting for age and APOE4 ($r\ (70) = 0.30$, $p < 0.05$), as well as with CERAD Delayed ($r\ (68) = 0.50$, $p < 0.001$), RAVLT delayed ($r\ (68) = 0.55$, $p < 0.001$), and RCFT delayed ($r\ (68) = 0.25$, $p < 0.05$).

Pattern of amyloid deposition based on principal components analysis

The KMO test of sampling adequacy yielded a value of 0.83 indicating the data was suitable for PCA. Three PCs were extracted accounting for 91.2% of the total variance. Initial eigenvalues indicated the first two extracted PCs accounted for 88.9% of the total variance. After the varimax rotation, the first two components explained 52.8% and 21.3% of the variance respectively, while PC3 accounted for 17%. PC1 was driven by mean SUVs of neocortical and striatal regions (Fig. 1). The highest loadings >0.85 came from the anterior cingulate, caudate nucleus, orbital frontal cortex, and middle frontal gyrus (Supplementary Table 2). Subcortical regions, including midbrain, medulla, cerebellum, pons, and thalamus, contributed mostly to PC2 (Supplementary Fig. 4). PC3 reflected SUVs of occipital lobe areas. Hippocampus, parahippocampus, and amygdala loaded on all PCs, with highest loadings of 0.7 on PC2.

Correlation between PCs and global CL\SUVR

A highly significant positive Pearson's correlation was found between with PC1 and global CLs ($r = 0.90$, $p = <0.0001$), Fig. 2A; a significant negative correlation with PC2 ($r = -0.27$, $p < 0.05$); and a significant positive correlation with PC3 ($r = 0.23$, $p < 0.05$; Supplementary Fig. 5).

Effects of APOE4, age, and education on principal components

A significant positive partial correlation was revealed between the presence of APOE4 and PC1 loadings ($r = 0.29$, $p < 0.05$). Years of education were significantly negatively correlated with PC1 after adjusting for age and APOE4 ($r = -0.26$, $p < 0.05$). Age did not significantly correlate with any of the extracted component loadings after controlling for APOE4 and years of education.

Blood plasma p-tau181

The p-tau181 concentration was significantly higher in the Aβ+ group (Table 1). A significant positive Pearson's correlation was found between PC1 and p-tau181 ($r = 0.46$, $p < 0.0001$; Fig. 2B). Using Aβ statuses with p-tau181 concentrations 27 individuals (36.9%) were classified as A−T− and 15 (20.5%) were A+T+. There were no differences in age, education or cognition for the AT groups (see Supplementary Table 1 for breakdown).

Correlation between cognitive measures and principal components

All cognitive tests indicated negative associations with PC1, but only the RCFT delayed score was significantly negatively correlated ($r = -0.27$, $p < 0.05$; Fig. 2C). Delayed CERAD was significantly negatively correlated with PC2 component loadings ($r = -0.25$, $p < 0.05$; Supplementary Fig. 6).

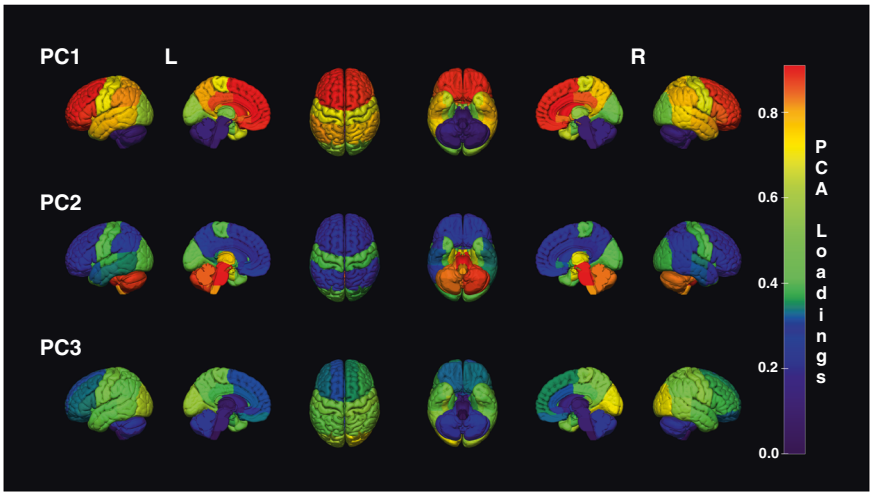

Fig. 1 Representation of regional loadings from the first three PCs. Each Hammers atlas region was scaled to its loading score from the PCA. The 3D rendering clearly demonstrates the highest loadings for PC1 were obtained in frontal neocortex, followed by striatum (see Supplementary Fig. 4). Highest loadings for PC2 were found in the brainstem and cerebellum, which are often reference regions for SUVR calculations. Highest loadings for PC3 were found in the occipital cortex. The same data are tabulated in Supplementary Table 2. Colour bar represents PC loadings from highest (red) to lowest (violet). PC principal component, L left, R right.

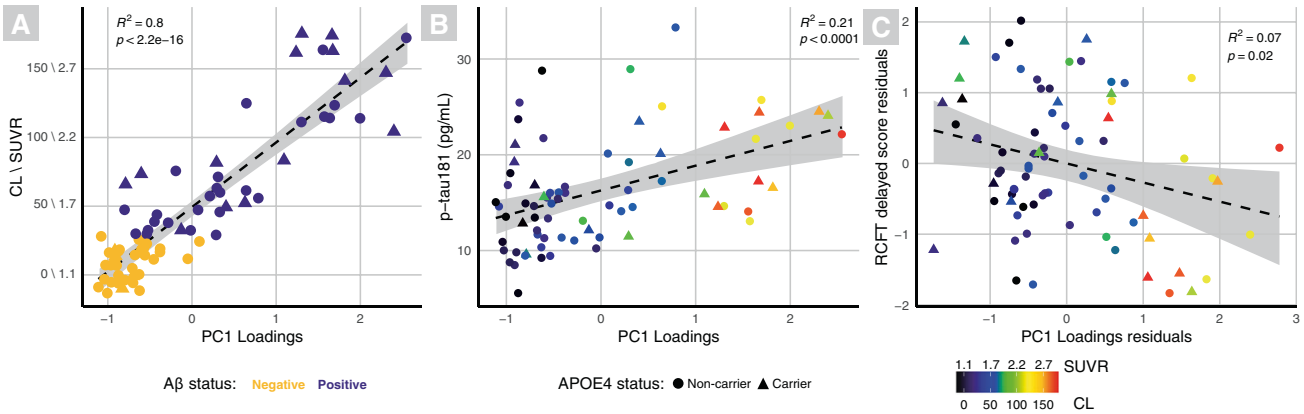

Fig. 2 Scatter plots displaying significant correlations with PC1. Each scatter plot shows a significant correlation between global CL \SUVRs and PC1 (**A**), blood plasma p-tau181 and PC1 (**B**), and the significant partial correlation (adjusted for age, years of education and APOE4) between delayed RCFT and PC1 (**C**). Triangles represent APOE4 carriers and circles APOE4 non-carriers. Binary Aβ status is depicted in **A** (Aβ− = yellow; Aβ+ = violet), **B**, **C** are coloured by continuous CL\SUVRs, represented by the colour bar.

In vivo staging schemes

Figure 3 depicts good correspondence between Aβ positivity (>29 CL, 53.3% of cohort) and combined high stages of staging schemes (Thal Phase 2 and 3, Grothe Stage III and IV, Mattsson stage 2 and 3). Binary classification into combined high or low stages showed 74 to 91% correspondence between schemes. Both CL and PC1 values provided good discrimination between high and low stages with areas under the receiver operating curves of 0.86 to 0.96. Substantial differences were noted for low stages between staging schemes. Thal's scheme classified 93.3% of the cohort as PET Aβ Phase estimate ≥1. Only 6.7% were Aβ- by Thal, 17.3% by Grothe and 28% by Mattsson. Grothe's scheme deemed 17.3% and Mattsson's 8.0% as unstageable, mostly in the low range of CL values (12–29 CL), which is considered the "grey zone" [35]. There was also little correspondence between CL and PC1 values at these low values (Fig. 2A).

Figure 4 depicts the spatial overlap between PC1, centiloid cortex, and the early/intermediate stages from in vivo schemes developed by Grothe [8] and Mattsson [11]. There is a clear regional overlap between all methods, largely within default mode network regions including anterior cingulate, orbital-, middle-, superior-frontal gyrus, posterior cingulate, and insula. Mattsson also classified the putamen as an intermediate amyloid accumulation region, which is relatable to the PCA showing comparable loadings of both neocortex and striatum on PC1. Regions of the centiloid cortical mask [34] also overlapped with PC1, particularly frontal, temporal, posterior cingulate and parietal cortices, but also the anterior striatum and insula. All the extracted PCs were significantly correlated with CLs derived from the centiloid cortex (Fig. 2B and Supplementary Fig. 5A, B).

DISCUSSION

This study used SUV-based PCA to investigate the regional pattern of amyloid deposition in a unique cohort of CU adults with a mean age of 85 years. It also applied three recently published in vivo Aβ staging schemes to the PET images. The PCA revealed three PCs based on mean ^{18}F-flutemetamol SUVs, indicative of differential amyloid burden in these areas. PC1 was driven by the large common variance of uptake in neocortical and striatal regions, PC2 represented non-specific uptake in typical reference regions for SUVR-based analyses, and PC3 represented the occipital lobe. The application of the Aβ staging schemes demonstrated that the

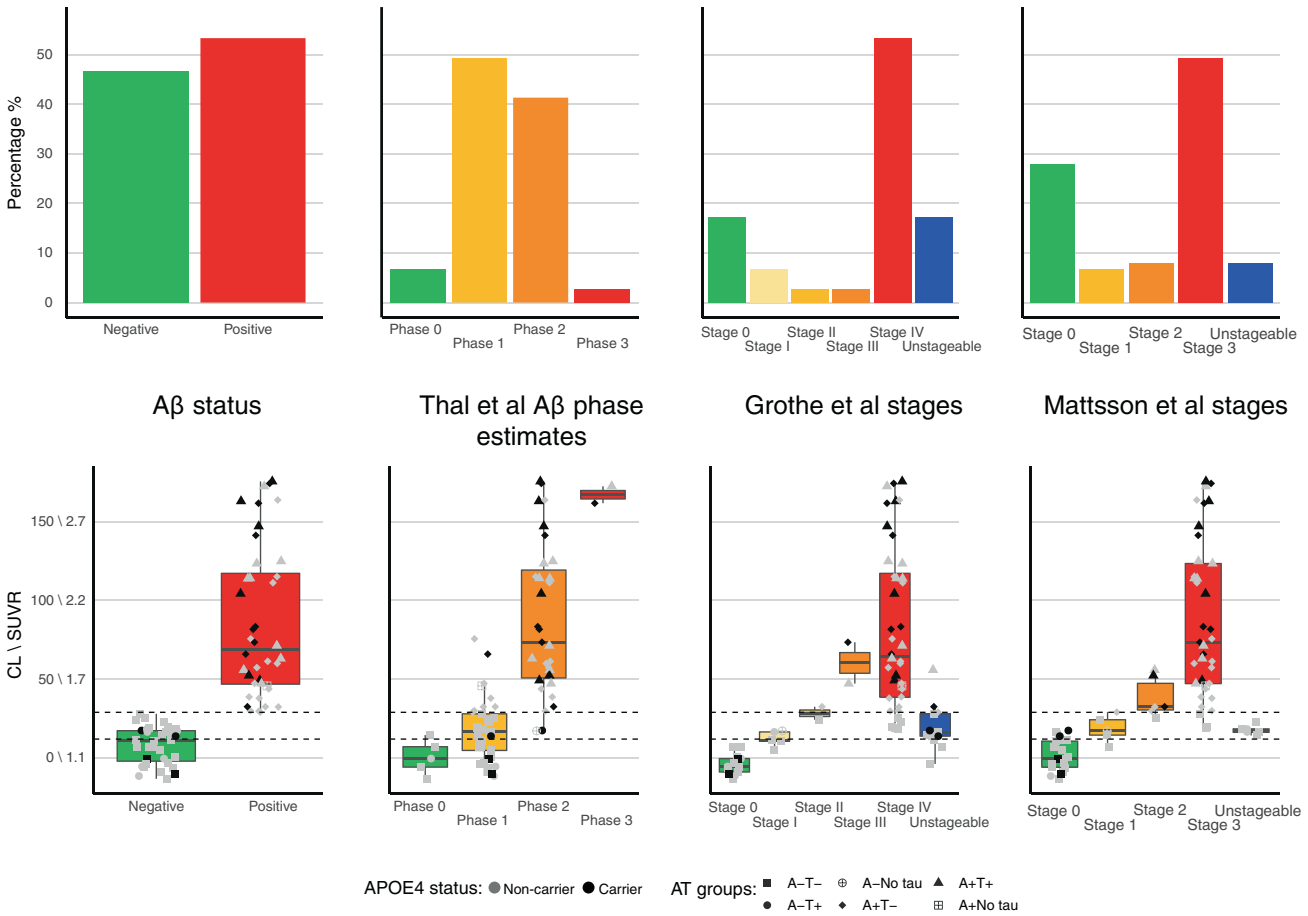

Fig. 3 Bar and box plots displaying the percentage of suprathreshold Aβ within brain regions defined by centiloid cortex and 3 in vivo amyloid staging schemes [7, 8, 11]. The top row shows the percentage of individuals categorised within each amyloid phase/stage, while the bottom row displays the global amyloid (CL\SUVR) for those individuals within each phase/stage. In the bottom row, shape of points represents AT status and colour of points represents APOE4 status (grey non-carriers and black carriers); dotted lines in the box plots represent the boundaries of the grey zone (12–29 CL). The figure demonstrates that independent of method, the majority of the cohort is categorised as having pathological quantities of Aβ. Each staging scheme reveals that those individuals at advanced stages tend to also have higher global CL\SUVRs.

majority of the cohort were classified as having pathological amount and distribution of Aβ.

The striatum (caudate/anterior putamen) was included in PC1, Mattsson [11], Klunk [34] and was also a key region in Thal's staging [7]. While the striatum is not regarded as an early amyloid accumulation region [8, 38], there was a tight covariation between neocortical and striatal regions in the current study, which might be related to the high age of the participants. It has been previously reported that older CU show advanced amyloid pathology including deposition in the striatum [14].

The current analysis did not use a reference region and was based on SUVs. Reference regions, such as pons and cerebellum, often used as a denominator in SUVRs, appeared within PC2. PC2 had a negative correlation with CL\SUVRs. Observing low variation and independence of PC2 from cortical regions, further supports using them as reference regions. Neocortical regions also had low loadings on PC2.

Occipital cortex showed highest PC3 loadings, indicating independent variation compared to neocortical and striatal areas. This could be explained by low occipital amyloid burden and conformational differences of amyloid deposits in the occipital lobe [39], especially since the occipital areas, including cuneus and lingual gyrus, are classified as late amyloid accumulation areas by Grothe's cross-sectional [8] and as intermediate by Mattsson's longitudinal staging schemes [11]. Participants with generally high amyloid load, either had high or low occipital load, which did not correlate with APOE4 status (Supplementary Fig. 7). Thus, a factor other than APOE4 may be governing amyloid accumulation in this region.

The APOE4 effect on increased ^{18}F-flutemetamol uptake in PC1 is consistent with previous research. APOE4 has been shown to increase amyloid burden in anterior cingulate, posterior cingulate, prefrontal, parietal and lateral temporal areas [40, 41]. These regions belong to well-established brain networks, including the default mode network, showing connectivity alterations and preferential amyloid accumulation in preclinical AD stages in asymptomatic APOE4+ individuals [42–45].

Although amyloid-cognition correlations are debated, some studies reveal a declining cognitive functioning linked to amyloid deposition, even in CU individuals [40, 46]. A weak, significant, negative partial correlation was found between the delayed RCFT and PC1 loadings (Fig. 2B). Worse RCFT performance, a visuospatial episodic memory test, has been linked to hypometabolism and cortical thinning of parietal, temporal, and frontal cortices [47, 48]. A FDG-PET-based PCA also demonstrated correlations between RCFT and metabolism in posterior cingulate, precuneus, parietal, lateral temporal, superior-frontal and medial prefrontal cortices [49]; all these regions loaded highly on PC1. Another weak but significant partial correlation was observed between CERAD delayed and PC2 loadings. Decreased GM density

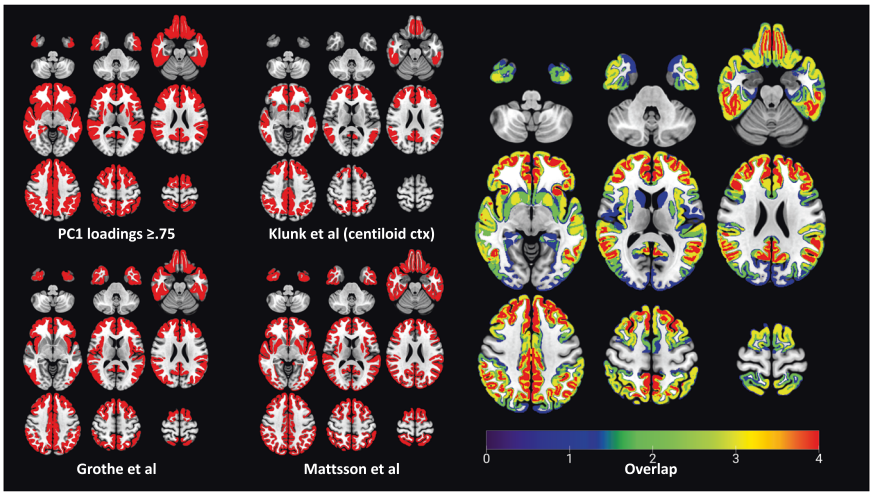

Fig. 4 Representation of early and moderate regional amyloid deposition by four different PET-based amyloid deposition schemes. The upper left figure depicts regions showing highest loadings for PC1 (≥0.75), including the frontal, parietal and temporal neocortex, caudate, and putamen. The bottom left figure illustrates stages I and II of the four-stage model of regional amyloid progression proposed by Grothe [8]. The upper middle figure shows cortical volume of interest from the centiloid method established by Klunk [34]. The bottom middle figure depicts the early and intermediate Aβ stages from the longitudinal CSF/PET staging proposed by Mattsson [11]. The brain rendering on the right illustrates the degree of regional overlap between these four methods, which the colour bar depicts; all four methods = red; single method = blue.

in regions with moderate loadings on PC2, such as the hippocampus, parahippocampal gyrus and thalamus, has been previously associated with worse CERAD immediate and delayed recall [50]. However, we did not find significant correlations between SUVRs of those regions and CERAD delayed.

Participants of this study were also categorised according to their Aβ deposition stage based on three schemes [7, 8, 11]. On a global level, 53.3% of the cohort were Aβ+ (CL >29) and 21.3% were in the "grey zone". Age-related factors need to be considered when assessing pathological deposits [51] because in non-demented elderly, older age can shift the amyloid distribution to higher values [52]. When applying Thal's methodology, which uses cortical and caudate SUVRs to stage individuals, 97.3% were at Aβ phase estimate 1 or above, with 44% in phase 2 or above. These phases would correspond to pathological quantities of Aβ post mortem. Although derived differently (frequency of Aβ positivity vs. longitudinal increases of Aβ), both Grothe and Mattsson's schemes had similar patterns with most individuals categorised in the latest stages (Stage IV and Stage 3; 53.3% and 49.3% respectively), with few individuals in the intermediate stages. Importantly, if the cut-offs used by Grothe (^{18}F-florbetapir SUVR of 0.92 converted to −21 CL using the published conversion [53]) and Mattsson (^{18}F-flutemetamol SUVRs of 0.738, 0.76 and 0.751 for Stages 1–3 respectively) were used on the current cohort, 100% would have been categorised in the highest stages (Stage IV and Stage 3).

This CU cohort is unique due to its high mean age of 85 years. The above-discussed staging schemes were created based on individuals who were on average at least 10 years younger. Risk factors for dementia differ in this age group when compared to younger elderly. Imaging biomarkers may also have limited applicability due to lower life expectancy and potential resilience to amyloid deposition [54]. Non-demented individuals at age of 85 years might show highly prevalent WM lesions, as well as global and hippocampal atrophy [55, 56]. Tau pathology also increases with age [57, 58] and although tau-PET was not available for the current cohort, plasma p-tau181 revealed a significant positive correlation between PC1 and p-tau181. Dichotomising amyloid-PET and plasma p-tau181 revealed 20.5% were classified as A+T+, thus having evidence of AD pathology without cognitive impairment. Previous multivariate analyses, including PCA, have been used to investigate the effects of age and amyloid on cognition in CU elderly [59]. Although dichotomous amyloid burden has been studied in the oldest-old, aged 85 years and more [2], there is limited neuroimaging research depicting detailed regional amyloid distribution in this old population. This study is novel because it not only assessed regional amyloid deposition, it also applied published in vivo amyloid staging schemes.

When aducanumab was initially approved for clinical use in the USA [60] the presence and removal of brain Aβ became a pressing and highly topical issue [61–63]. It is still unclear whether pathological brain Aβ is as relevant at advanced ages because many Aβ+ oldest-old will never develop cognitive impairment or dementia in their lifetime. This is important because administering a monoclonal antibody to a person who does not need it, is not only expensive but can actually cause harm (e.g., ARIA-E). The present data indicates the uncertainty whether the hierarchal, regional progression patterns based on the in vivo PET staging can be applied cross-sectionally to oldest-old cohorts, and whether positivity cut-offs established on younger populations apply in the ninth and tenth decades of life. Therefore, an open question remains about what constitutes abnormal Aβ in the oldest-old and whether Aβ should be removed from such people's brains.

This study has limitations. The cross-sectional nature of the data does not allow for conclusions on causal relationships between the variables. Longitudinal research would be essential for assessing the relationship between increasing age, cognitive decline, and progressive changes in Aβ deposition. Due to the data-driven nature of PCA, the modest sample size, as well as the old age of the participants, it's unclear whether the extracted PCs would generalise to independent younger or diseased cohorts. Moreover, findings based on ^{18}F-flutemetamol PET data are only a proxy for actual Aβ neuropathology. Finally, the PCA was conducted on mean regional SUVs, which are dependent on the accurate placement of the regions of interest but are less confounded by noise than voxel-wise PCA [64].

In conclusion, although PC1 and staging schemes broadly overlapped, there was poor correspondence between schemes with respect to early Aβ stages based on regional thresholds. The PCA demonstrated concurrent accumulation across striatum and most cortical regions (apart from hippocampus and occipital cortex), which contrasts with sequential regional accumulation proposed by staging

schemes. The data also indicate that a large proportion (up to 93%) of CU elderly have brain Aβ deposits classified as pathological by in vivo PET staging schemes. The study therefore raises important questions about the utility of staging, as opposed to binarising, amyloid-PET from a single scan in the oldest-old, what constitutes abnormal brain Aβ in this age group, and what, if anything, should be done therapeutically for PET Aβ+ CU individuals 85 years of age and above?

DATA AVAILABILITY

Requests from suitably qualified individuals for data supporting the findings of this study will be considered by the corresponding author and subject to a data transfer agreement with the host university (University of Manchester).

REFERENCES

1. Jack CR Jr., Knopman DS, Jagust WJ, Petersen RC, Weiner MW, Aisen PS, et al. Tracking pathophysiological processes in Alzheimer's disease: an updated hypothetical model of dynamic biomarkers. Lancet Neurol. 2013;12:207–16.
2. Jansen WJ, Ossenkoppele R, Knol DL, Tijms BM, Scheltens P, Verhey FR, et al. Prevalence of cerebral amyloid pathology in persons without dementia: a meta-analysis. JAMA. 2015;313:1924–38.
3. Hameed S, Fuh J-L, Senanarong V, Ebenezer EGM, Looi I, Dominguez J, et al. Role of fluid biomarkers and PET imaging in early diagnosis and its clinical implication in the management of Alzheimer's disease. J Alzheimer's Dis Rep. 2020;4:1–17.
4. Salloway S, Gamez JE, Singh U, Sadowsky CH, Villena T, Sabbagh MN, et al. Performance of [18F] flutemetamol amyloid imaging against the neuritic plaque component of CERAD and the current (2012) NIA-AA recommendations for the neuropathologic diagnosis of Alzheimer's disease. Alzheimer's Dement: Diagn Assess Dis Monit. 2017;9:25–34.
5. Thal DR, Rüb U, Orantes M, Braak H. Phases of Aβ-deposition in the human brain and its relevance for the development of AD. Neurology. 2002;58:1791–800.
6. Cho H, Choi JY, Hwang MS, Kim YJ, Lee HM, Lee HS, et al. In vivo cortical spreading pattern of tau and amyloid in the Alzheimer disease spectrum. Ann Neurol. 2016;80:247–58.
7. Thal DR, Beach TG, Zanette M, Lilja J, Heurling K, Chakrabarty A, et al. Estimation of amyloid distribution by [18 F] flutemetamol PET predicts the neuropathological phase of amyloid β-protein deposition. Acta Neuropathol. 2018;136:557–67.
8. Grothe MJ, Barthel H, Sepulcre J, Dyrba M, Sabri O, Teipel SJ, et al. In vivo staging of regional amyloid deposition. Neurology. 2017;89:2031–8.
9. Jelistratova I, Teipel SJ, Grothe MJ. Longitudinal validity of PET-based staging of regional amyloid deposition. Hum Brain Mapp. 2020;41:4219–31.
10. Sakr FA, Grothe MJ, Cavedo E, Jelistratova I, Habert M-O, Dyrba M, et al. Applicability of in vivo staging of regional amyloid burden in a cognitively normal cohort with subjective memory complaints: the INSIGHT-preAD study. Alzheimer's Res Ther. 2019;11:1–11.
11. Mattsson N, Palmqvist S, Stomrud E, Vogel J, Hansson O. Staging β-amyloid pathology with amyloid positron emission tomography. JAMA Neurol. 2019;76:1319–29.
12. Teipel SJ, Temp AG, Levin F, Dyrba M, Grothe MJ, Initiative AsDN. Association of PET-based stages of amyloid deposition with neuropathological markers of Aβ pathology. Ann Clin Transl Neurol. 8:29–42;2021.
13. Wolf DS, Gearing M, Snowdon DA, Mori H, Markesbery WR, Mirra SS. Progression of regional neuropathology in Alzheimer disease and normal elderly: findings from the Nun study. Alzheimer Dis Assoc Disord. 1999;13:226–31.
14. Beker N, Ganz A, Hulsman M, Klausch T, Schmand BA, Scheltens P, et al. Association of cognitive function trajectories in centenarians with postmortem neuropathology, physical health, and other risk factors for cognitive decline. JAMA Netw Open. 2021;4:e2031654.
15. Habeck C, Stern Y. Multivariate data analysis for neuroimaging data: overview and application to Alzheimer's disease. Cell Biochem Biophys. 2010;58:53–67.
16. Zuendorf G, Kerrouche N, Herholz K, Baron JC. Efficient principal component analysis for multivariate 3D voxel-based mapping of brain functional imaging data sets as applied to FDG-PET and normal aging. Hum Brain Mapp. 2003;18:13–21.
17. Kerrouche N, Herholz K, Mielke R, Holthoff V, Baron J-C. 18FDG PET in vascular dementia: differentiation from Alzheimer's disease using voxel-based multivariate analysis. J Cereb Blood Flow Metab. 2006;26:1213–21.
18. Fripp J, Bourgeat P, Acosta O, Raniga P, Modat M, Pike KE, et al. Appearance modeling of 11C PiB PET images: characterizing amyloid deposition in Alzheimer's disease, mild cognitive impairment and healthy aging. Neuroimage. 2008;43:430–9.
19. Lilja J, Leuzy A, Chiotis K, Savitcheva I, Sörensen J, Nordberg A. Spatial normalization of 18F-flutemetamol PET images using an adaptive principal-component template. J Nucl Med. 2019;60:285–91.
20. Robinson AC, Davidson YS, Horan MA, Pendleton N, Mann D. Pathological correlates of cognitive impairment in the University of Manchester longitudinal study of cognition in normal healthy old age. J Alzheimer's Dis. 2018;64:483–96.
21. Konijnenberg E, Carter SF, Ten Kate M, Den Braber A, Tomassen J, Amadi C, et al. The EMIF-AD PreclinAD study: study design and baseline cohort overview. Alzheimer's Res Ther. 2018;10:75.
22. Keller SH, Svarer C, Sibomana M. Attenuation correction for the HRRT PET-scanner using transmission scatter correction and total variation regularization. IEEE Trans Med Imaging. 2013;32:1611–21.
23. Sibomana M, Byars L, Panin V, Lenox M, Kehren F, Rist J, et al. Simultaneous measurement of transmission and emission contamination using a collimated /sup 137/Cs point source for the HRRT. Nuclear Science Symposium Conference Record, 2004 IEEE. 2004;4:2647–51.
24. Sureau FC, Reader AJ, Comtat C, Leroy C, Ribeiro MJ, Buvat I, et al. Impact of image-space resolution modeling for studies with the high-resolution research tomograph. J Nucl Med. 2008;49:1000–8.
25. Comtat C, Sureau FC, Sibomana M, Hong IK, Sjoholm N, Trebossen R. Image based resolution modeling for the HRRT OSEM reconstructions software. Proceedings of the 2008 IEEE Nuclear Science Symposium Conference Record; 19–25 Oct. 2008. p. 4120–3. https://doi.org/10.1109/NSSMIC.2008.4774188.
26. Hudson HM, Larkin RS. Accelerated image reconstruction using ordered subsets of projection data. IEEE Trans Med Imaging. 1994;13:601–9.
27. Hong IK, Chung ST, Kim HK, Kim YB, Son YD, Cho ZH. Ultra fast symmetry and SIMD-based projection-backprojection (SSP) algorithm for 3-D PET image reconstruction. IEEE Trans Med Imaging. 2007;26:789–803.
28. Ashton NJ, Pascoal TA, Karikari TK, Benedet AL, Lantero-Rodriguez J, Brinkmalm G, et al. Plasma p-tau231: a new biomarker for incipient Alzheimer's disease pathology. Acta Neuropathol. 2021;141:709–24.
29. Karikari TK, Pascoal TA, Ashton NJ, Janelidze S, Benedet AL, Rodriguez JL, et al. Blood phosphorylated tau 181 as a biomarker for Alzheimer's disease: a diagnostic performance and prediction modelling study using data from four prospective cohorts. Lancet Neurol. 2020;19:422–33.
30. Karikari TK, Benedet AL, Ashton NJ, Lantero Rodriguez J, Snellman A, Suarez-Calvet M, et al. Diagnostic performance and prediction of clinical progression of plasma phospho-tau181 in the Alzheimer's disease neuroimaging initiative. Mol Psychiatry. 2021;26:429–42.
31. Hammers A, Chen CH, Lemieux L, Allom R, Vossos S, Free SL, et al. Statistical neuroanatomy of the human inferior frontal gyrus and probabilistic atlas in a standard stereotaxic space. Hum Brain Mapp. 2007;28:34–48.
32. Desikan RS, Segonne F, Fischl B, Quinn BT, Dickerson BC, Blacker D, et al. An automated labeling system for subdividing the human cerebral cortex on MRI scans into gyral based regions of interest. Neuroimage. 2006;31:968–80.
33. Ashburner J. A fast diffeomorphic image registration algorithm. Neuroimage. 2007;38:95–113.
34. Klunk WE, Koeppe RA, Price JC, Benzinger TL, Devous Sr MD, Jagust WJ, et al. The Centiloid Project: standardizing quantitative amyloid plaque estimation by PET. Alzheimer's Dement. 2015;11:1–15. e14.
35. Salvado G, Molinuevo JL, Brugulat-Serrat A, Falcon C, Grau-Rivera O, Suarez-Calvet M, et al. Centiloid cut-off values for optimal agreement between PET and CSF core AD biomarkers. Alzheimers Res Ther. 2019;11:27.
36. La Joie R, Ayakta N, Seeley WW, Borys E, Boxer AL, DeCarli C, et al. Multisite study of the relationships between antemortem [(11)C]PIB-PET Centiloid values and postmortem measures of Alzheimer's disease neuropathology. Alzheimers Dement. 2019;15:205–16.
37. Beaumont R. An introduction to principal component analysis & factor analysis using SPSS 19 and R (psych package). Factor Analysis and Principal Component Analysis (PCA). 2012;24.
38. Fantoni E, Collij L, Alves IL, Buckley C, Farrar G. The spatial-temporal ordering of amyloid pathology and opportunities for PET imaging. J Nucl Med. 2020;61:166–71.
39. Rasmussen J, Mahler J, Beschorner N, Kaeser SA, Hasler LM, Baumann F, et al. Amyloid polymorphisms constitute distinct clouds of conformational variants in different etiological subtypes of Alzheimer's disease. Proc Natl Acad Sci USA 2017;114:13018–23.
40. Rodrigue K, Kennedy K, Devous M, Rieck J, Hebrank A, Diaz-Arrastia R, et al. β-Amyloid burden in healthy aging: regional distribution and cognitive consequences. Neurology. 2012;78:387–95.
41. Kang DW, Wang S-M, Na H-R, Lee CU, Baek I-H, Lim HK. Differential effects of the interaction between the education and APOE ε4 allele on amyloid-beta retention and memory performances in cognitively normal older adults and Alzheimer's disease patients. Curr Alzheimer Res. 2020;17:1023–32.

42. Goryawala M, Duara R, Loewenstein DA, Zhou Q, Barker W, Adjouadi M, et al. Apolipoprotein-E4 (ApoE4) carriers show altered small-world properties in the default mode network of the brain. Biomed Phys Eng Express. 2015;1:015001.
43. Wu X, Li Q, Yu X, Chen K, Fleisher AS, Guo X, et al. A triple network connectivity study of large-scale brain systems in cognitively normal APOE4 carriers. Front Aging Neurosci. 2016;8:231.
44. Palmqvist S, Schöll M, Strandberg O, Mattsson N, Stomrud E, Zetterberg H, et al. Earliest accumulation of β-amyloid occurs within the default-mode network and concurrently affects brain connectivity. Nat Commun. 2017;8:1–13.
45. Quevenco FC, van Bergen JM, Treyer V, Studer ST, Kagerer SM, Meyer R, et al. Functional brain network connectivity patterns associated with normal cognition at old-age, local β-amyloid, Tau, and APOE4. Front Aging Neurosci. 2020;12:46.
46. Hammers DB, Atkinson TJ, Dalley BC, Suhrie KR, Horn KP, Rasmussen KM, et al. Amyloid positivity using [18F] flutemetamol-PET and cognitive deficits in non-demented community-dwelling older adults. Am J Alzheimer's Dis Other Dement®. 2017;32:320–8.
47. Melrose RJ, Harwood D, Khoo T, Mandelkern M, Sultzer DL. Association between cerebral metabolism and Rey–Osterrieth complex figure test performance in Alzheimer's disease. J Clin Exp Neuropsychol. 2013;35:246–58.
48. Ahn H-J, Seo SW, Chin J, Suh MK, Lee BH, Kim ST, et al. The cortical neuroanatomy of neuropsychological deficits in mild cognitive impairment and Alzheimer's disease: a surface-based morphometric analysis. Neuropsychologia. 2011;49:3931–45.
49. Salmon E, Kerrouche N, Perani D, Lekeu F, Holthoff V, Beuthien-Baumann B, et al. On the multivariate nature of brain metabolic impairment in Alzheimer's disease. Neurobiol Aging. 2009;30:186–97.
50. Santos VD, Thomann PA, Wüstenberg T, Seidl U, Essig M, Schröder J. Morphological cerebral correlates of CERAD test performance in mild cognitive impairment and Alzheimer's disease. J Alzheimer's Dis. 2011;23:411–20.
51. Nelson PT, Alafuzoff I, Bigio EH, Bouras C, Braak H, Cairns NJ, et al. Correlation of Alzheimer disease neuropathologic changes with cognitive status: a review of the literature. J Neuropathol Exp Neurol. 2012;71:362–81.
52. Chiotis K, Carter SF, Farid K, Savitcheva I, Nordberg A. Amyloid PET in European and North American cohorts; and exploring age as a limit to clinical use of amyloid imaging. Eur J Nucl Med Mol imaging. 2015;42:1492–506.
53. Navitsky M, Joshi AD, Kennedy I, Klunk WE, Rowe CC, Wong DF, et al. Standardization of amyloid quantitation with florbetapir standardized uptake value ratios to the Centiloid scale. Alzheimers Dement. 2018;14:1565–71.
54. Kawas CH, Legdeur N, Corrada MM. What have we learned from cognition in the oldest-old. Curr Opin Neurol. 2021;34:258–65.
55. Woodworth DC, Scambray KA, Corrada MM, Kawas CH, Sajjadi SA. Neuroimaging in the oldest-old: a review of the literature. J Alzheimers Dis. 2021;82:129–47.
56. Snitz BE, Weissfeld LA, Lopez OL, Kuller LH, Saxton J, Singhabahu DM, et al. Cognitive trajectories associated with beta-amyloid deposition in the oldest-old without dementia. Neurology. 2013;80:1378–84.
57. Braak H, Braak E. Frequency of stages of Alzheimer-related lesions in different age categories. Neurobiol Aging. 1997;18:351–7.
58. Scholl M, Lockhart SN, Schonhaut DR, O'Neil JP, Janabi M, Ossenkoppele R, et al. PET imaging of Tau deposition in the aging human brain. Neuron. 2016;89:971–82.
59. Oh H, Madison C, Haight TJ, Markley C, Jagust WJ. Effects of age and beta-amyloid on cognitive changes in normal elderly people. Neurobiol Aging. 2012;33:2746–55.
60. Mullard A. Landmark Alzheimer's drug approval confounds research community. Nature. 2021;594:309–10.
61. Karlawish J, Grill JD. The approval of Aduhelm risks eroding public trust in Alzheimer research and the FDA. Nat Rev Neurol. 2021;17:523–4.
62. Liu KY, Howard R. Can we learn lessons from the FDA's approval of aducanumab? Nat Rev Neurol. 2021;17:715–22.
63. Selkoe DJ. Treatments for Alzheimer's disease emerge. Science. 2021;373:624–6.
64. Martens C, Debeir O, Decaestecker C, Metens T, Lebrun L, Leurquin-Sterk G, et al. Voxelwise principal component analysis of dynamic [S-Methyl-(11)C]Methionine PET data in glioma patients. Cancers. 2021;13:2342.

ACKNOWLEDGEMENTS

This work received financial support from the EU/EFPIA Innovative Medicines Initiative Joint Undertaking EMIF grant agreement no. 115372. This work also received in-kind sponsoring from GE Healthcare in the form of flutemetamol cassettes for production of the radiotracer at the Wolfson Molecular Imaging Centre using GE's FASTlab system. This work has also been supported by the Erasmus+ programme of the European Union. The European Commission support for the production of this publication does not constitute an endorsement of the contents which reflects the views only of the authors, and the Commission cannot be held responsible for any use which may be made of the information contained therein. SFC is supported by the NIHR Cambridge Biomedical Research Centre (BRC-1215-20014). The views expressed are those of the authors and not necessarily those of the NIHR or the Department of Health and Social Care. We are very grateful to the individuals who participated in this study and their long dedication to ageing research. This study also would not have been possible without operational support colleagues at the Wolfson Molecular Imaging Centre and the research nurses and radiographers at the NIHR Manchester Clinical Research Facility within Manchester Royal Infirmary.

AUTHOR CONTRIBUTIONS

All authors made substantial contributions to the creation of the work and approved the final version to be published. Conceptualisation: KH, MMM, SFC, and RH; Data acquisition/processing: JMA-R, CA, LM, NP, RH, NJA, and SFC; Data analysis: MMM and SFC; Writing—draft preparation: MMM; Writing—review and editing: KH, RH, SFC, NJA, TKK, KB, and HZ; Visualisation: SFC; Supervision: KH, RH, and SFC; Funding acquisition: NP and KH.

COMPETING INTERESTS

NJA has given lectures in symposia sponsored by Eli Lilly. KB has served as a consultant, at advisory boards, or at data monitoring committees for Abcam, Axon, BioArctic, Biogen, JOMDD/Shimadzu. Julius Clinical, Lilly, MagQu, Novartis, Ono Pharma, Pharmatrophix, Prothena, Roche Diagnostics, and Siemens Healthineers, and is a co-founder of Brain Biomarker Solutions in Gothenburg AB (BBS), which is a part of the GU Ventures Incubator Program, outside the work presented in this paper. HZ has served at scientific advisory boards and/or as a consultant for Abbvie, Alector, Annexon, Artery Therapeutics, AZTherapies, CogRx, Denali, Eisai, Nervgen, Novo Nordisk, Pinteon Therapeutics, Red Abbey Labs, Passage Bio, Roche, Samumed, Siemens Healthineers, Triplet Therapeutics, and Wave, has given lectures in symposia sponsored by Cellectricon, Fujirebio, Alzecure, Biogen, and Roche, and is a co-founder of Brain Biomarker Solutions in Gothenburg AB (BBS), which is a part of the GU Ventures Incubator Program (outside submitted work). The remaining authors declare no conflicts of interest.

ETHICS APPROVAL AND CONSENT TO PARTICIPATE

The study was approved by the Greater Manchester South Research Ethics Committee (ref: 14/NW/011). The participants provided written informed consent at the time of inclusion in the PreclinAD study from the European Medical Information Framework for AD (EMIF-AD). Previously published study providing details of recruitment and ethical considerations has been cited.

ADDITIONAL INFORMATION

Supplementary information The online version contains supplementary material available at https://doi.org/10.1038/s41380-022-01685-6.

Correspondence and requests for materials should be addressed to Stephen F. Carter.

Reprints and permission information is available at http://www.nature.com/reprints

Publisher's note Springer Nature remains neutral with regard to jurisdictional claims in published maps and institutional affiliations.